Journal of Organometallic Chemistry 897 (2019) 236–246

Contents lists available at ScienceDirect

Journal of Organometallic Chemistry

journal homepage: www.elsevier.com/locate/jorganchem

Copper-catalyzed Mizoroki-Heck coupling reaction using an efficient and magnetically reusable Fe_3O_4@SiO_2@PrNCu catalyst

Issa Yavari [a], Akbar Mobaraki [a, *], Zhila Hosseinzadeh [b], Nader Sakhaee [c]

[a] Department of Chemistry, Tarbiat Modarres University, P.O. Box. 14115-175, Tehran, Iran
[b] Department of Chemistry, K. N. Toosi University of Technology, Tehran, Iran
[c] Department of Chemistry, Harris-Stowe State University, St. Louis, USA

ARTICLE INFO

Article history:
Received 23 January 2019
Received in revised form
19 June 2019
Accepted 22 June 2019
Available online 26 June 2019

Keywords:
Magnetic
Heterogeneous catalyst
Copper
Coupling reaction

ABSTRACT

This study intends to design and prepare a new magnetic copper catalyst and its activity was assessed by carbon-carbon coupling reactions. For this purpose, 1-[3-(trimethoxysilyl) propyl] urea (TMSPU), hydrazine and CuI were used sequentially to modify Fe_3O_4@SiO_2 core-shell magnetic nanoparticles to obtain an efficient magnetic transition metal catalyst. Various analytical techniques were used to characterize the catalyst to show that the achieved structure and its properties are well-suited for coupling reactions. Finally, Mizoroki-Heck and Ullmann coupling reactions were performed using Fe_3O_4@SiO_2@PrNCu catalyst. The new catalyst offer simple synthetic procedure, convenient use for routine casework and low price. The Fe_3O_4@SiO_2@PrNCu catalyst was easily separated by means of a permanent and ordinary magnet and the recovered catalyst was reused in six cycles without any significant loss of activity.

1. Introduction

Regarding both industrial and synthetic point of views, transition-metal catalyzed carbon–carbon coupling reaction is a fundamental and challenging process since substitution reactions can occur on planar centers [1]. Carbon–carbon coupling reactions are included broadly in the synthetic procedures of valuable compounds such as various polymers, agrochemicals, dyes, organic conductors/semi-conductors and pharmaceutical intermediates [2,3]. Although our predecessors developed kinds of coupling reactions in recent decades but for large scale applications significant concern and drawbacks of this type of chemistry still remained that are the costs of the metal and ligand as well as the need for fully removing the metal from the final products.

So to overcome these drawbacks, as the first step, due to the high surface to volume ratios and very active surface atoms, transition-metal nanoparticles are very attractive catalysts compared to bulk catalysts [4]. Also, the design and/or utilization of organic ligands with carefully-placed binding sites offer great potential for the manufacture of complexes with novel architectures. In this regard, several chelators such as diamines, amino acids, 1,10-phenantrolines, diols and other nitrogen-, phosphorus- and oxygen-containing ligands are of a high interest because of their complexation and the chelation affinity [5]. Therefore, using different grafted electron-rich ligands in order to anchor the transition-metal nanoparticles, can address the second draw-back. Finally, to achieve optimal recyclability of the catalytic systems various studies on the magnetic character and catalytic applicability of the FeM magnetic nanoparticles were considered to overcome the third drawback [6]. In this case, hybrid organic–inorganic materials based on Fe_3O_4@SiO_2 core–shell magnetic nanoparticles as special immobilizing carrier of the catalyst' active sites have made significant contribution to current researches [6–8]. This is due to their inherent properties such as easy renewability and recovery by magnetic separation, thermal stability against degradation, large surface area and higher loading of metal-ligand complexes. The recent demand for low-cost and sustainable reaction procedures made many researchers turn their attention to design the new copper-mediated coupling reactions [5,9]. Among the carbon–carbon coupling reactions, Ullmann coupling of aryl halides offers resourceful ways of large-scale constructing biaryl units in some industrial processes [5,10]. While significant improvement in this area has been made, using a variety of

* Corresponding author.
E-mail addresses: yavarisa@modares.ac.ir (I. Yavari), akbar.mobaraki@gmail.com (A. Mobaraki), j.hosseinzadeh44@gmail.com (Z. Hosseinzadeh), SakhaeeN@hssu.edu (N. Sakhaee).

https://doi.org/10.1016/j.jorganchem.2019.06.029
0022-328X/

transition-metal catalysts, the great numbers of reported Ullmann protocols are still homogeneous and the effective reports on heterogeneous and recyclable catalytic methods are inadequate [5,11]. Therefore, there has been remarkable attention in developing novel heterogeneous catalytic systems for this process with efficient reusability while preserving the basic activity of the catalytic active sites. In order to identify a robust and easily prepared system to catalyze carbon–carbon bond-forming reactions, we have designed, prepared and characterized Fe_3O_4@SiO_2@PrNCu as an active heterogeneous magnetic catalyst (Scheme 1) and investigate its applicability in Ullmann carbon–carbon coupling reaction.

2. Material and methods

2.1. Generals

All the chemicals used in our prepared magnetic transition-metal catalyst achieved from several accomplished experiments were purchased at Merck and Aldrich Chemical Companies. The magnetic transition-metal catalyst was characterized by means of powder X-ray diffraction (XRD), transmission electron microscopy (TEM), Fourier transformed infrared spectroscopy (FT-IR) and energy dispersive X-ray analysis (EDX). FT-IR spectrum was acquired with an ABB Bomem Model FTLA 2000 spectrophotometer using KBr disc at room temperature. To demonstrate the texture and particle sizes of the magnetic transition-metal catalyst Fe_3O_4@SiO_2@PrNCu, transmission electron microscopy (TEM) images were taken with a Philips CM-10 instrument. The magnetic sample was prepared as the result of placing a drop of dilute nanoparticle solution on a carbon-coated copper grid, and drying in vacuum at room temperature overnight. The crystalline structure of the magnetic transition-metal catalyst was investigated with XRD pattern with a Philips X'Pert MPD Holland X-ray diffractometer with Co-Kα radiation, with accelerating voltage and current of 40 kV and 40 mA, respectively. EDX analysis for measuring the elements was performed with using an environmental scanning electron microscope Philips XL30 analyzer. The magnetization curve of the catalyst was measured at room temperature with applying a magnetic field of 15 kOe using vibrating sample magnetometer.

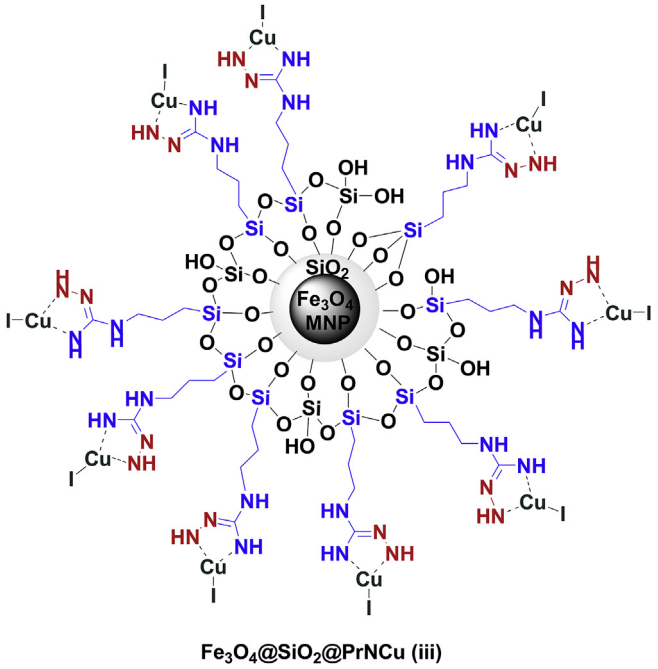

Fe_3O_4@SiO_2@PrNCu (iii)

Scheme 1. Schematic representation of the prepared magnetic transition-metal catalyst, Fe_3O_4@SiO_2@PrNCu.

2.2. Preparation of the Fe_3O_4 MNPs (i)

Preparation of Fe_3O_4 MNPs was performed by using the procedure rendered by Luo and co-workers [12]. In this procedure, Fe salts, ferrous chloride tetrahydrate $FeCl_2 \cdot 4H_2O$ (4.0 g, 20.1 mmol) and ferric chloride hexahydrate $FeCl_3 \cdot 6H_2O$ (11.0 g, 40.7 mmol) were dissolved in deionized water (250 mL) under nitrogen atmosphere with mechanical stirrer at 85 °C. Using aqueous NH_3 (25%), the pH value of the solution was adjusted to 9–11. After a continuous stirring for 4 h, for descending of pH value until 7.0, magnetite precipitates were washed with distilled water. A black precipitate (Fe_3O_4) was eventually collected with an external magnet at the bottom of the reaction flask (Scheme 2).

2.3. Preparation of the core-shell Fe_3O_4@SiO_2 MNPs (ii)

The silica coated core-shell magnetic nanoparticles (Fe_3O_4@SiO_2 MNPs) were prepared with an ultrasonic premixing of a dispersion of the Fe_3O_4 black precipitate (2.0 g) in ethanol (400 mL) for approximately 30 min at 25 °C temperature. Then, aqueous NH_3 (25%, 12 mL) and TEOS (4.0 mL) were slowly added successively. The resulting solution was mechanically stirred continuously for 24 h, after which the black precipitate product (Fe_3O_4@SiO_2) was collected by a simple magnet and washed with ethanol (3× 15 mL) and dried under vacuum overnight at room temperature (Scheme 2).

2.4. Preparation of the Fe_3O_4@SiO_2@PrNCu (iii)

The surface functionalization of the silica coated core-shell magnetic nanoparticles (Fe_3O_4@SiO_2 MNPs) with a guanidine like ligand was involved a synthetic strategy based on a grafting of 1-[3-(trimethoxysilyl) propyl] urea (TMSPU) precursor on the Fe_3O_4@SiO_2 MNPs. In a typical preparation procedure, TMSPU (0.60 g, 2.7 mmol), hydrazine (0.20 g, 4.0 mmol) and CuI (0.76 g, 4.0 mmol) were added subsequently to dry toluene (35 mL) containing silica-coated magnetic nanoparticles (1.0 g). The resulting mixture was stirred for 24 h and washed with toluene (2 × 15 mL) and several times with ethanol and eventually dried at room temperature under vacuum overnight to give the corresponding magnetic transition-metal catalyst Fe_3O_4@SiO_2@PrNCu (iii) (Scheme 2).

2.5. General procedure for the Ullmann reaction

A mixture of aryl halide (2.0 mmol), K_3PO_4 (3 mmol) and Fe_3O_4@SiO_2@PrNCu magnetic transition-metal catalyst (1 mol%) in 3 mL water were stirred at 100 °C for an appropriate time (Table 4). The progress of the reaction was monitored by TLC. After completion of the reaction, the mixture was cooled to room temperature and poured into H_2O (10 ml), and extracted with CH_2Cl_2 (2 × 5 ml) to separate the catalyst from the product by magnetic decantation. After extraction, the organic layer was dried over anhydrous Na_2SO_4 and concentrated under reduced pressure; the residue was subjected to column chromatography on silica gel (ethyl acetate and hexane as eluent) to yield the expected pure product. All products were characterized by ^1H and ^{13}C spectra (refer to electronic supporting information).

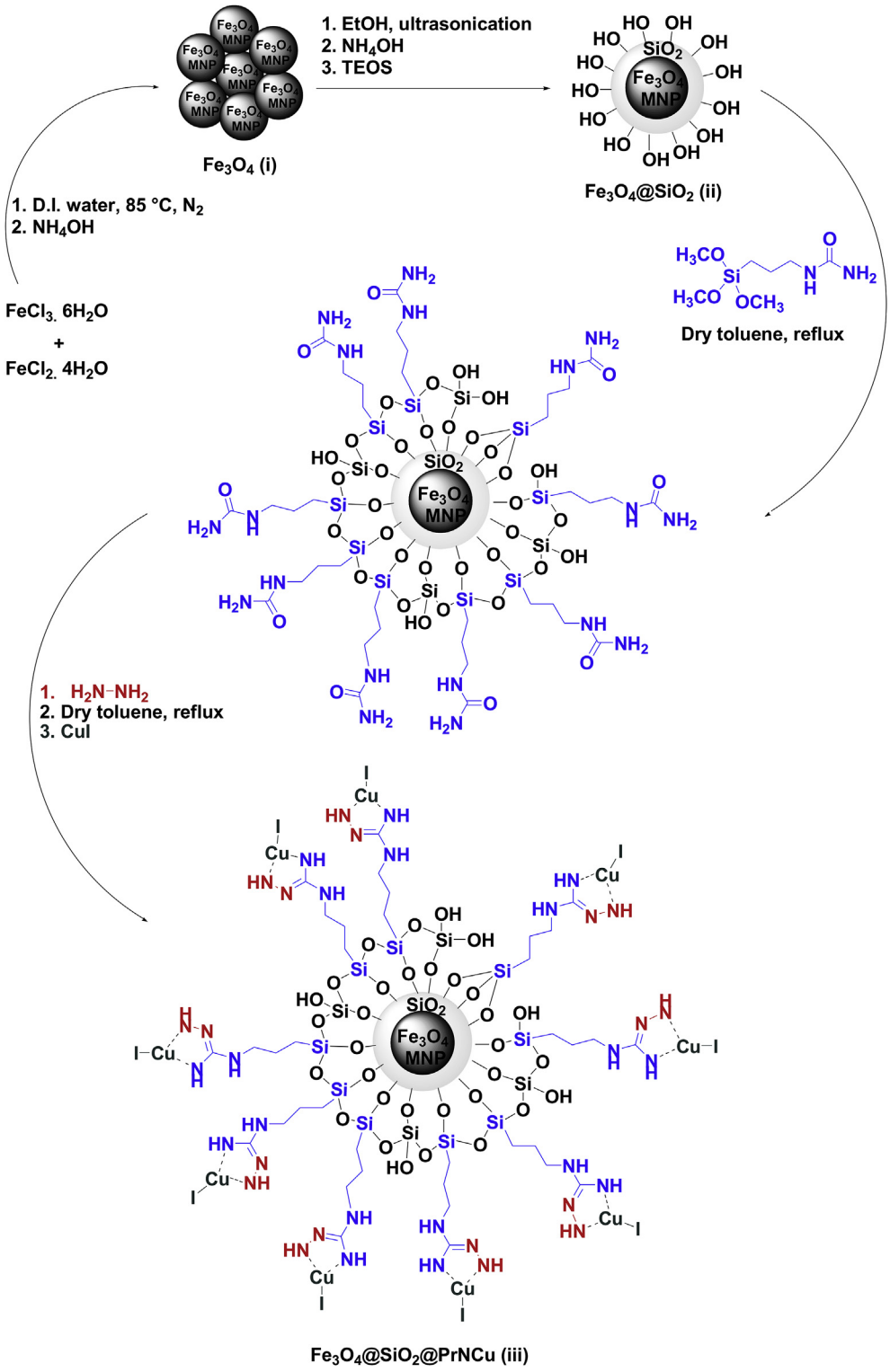

Scheme 2. Synthetic scheme of the Fe_3O_4 (i), Fe_3O_4@SiO_2 (ii) and Fe_3O_4@SiO_2@PrNCu (iii).

2.6. General procedure for the Mizoroki-Heck reaction

A mixture of aryl halide (1.0 mmol), alkene (1.2 mmol), K_3PO_4 (2 mmol), [For some electron deficient aryl halides, TBAB (0.5–1.0 mmol) was also added] and Fe_3O_4@SiO_2@PrNCu magnetic transition-metal catalyst (0.2 mol%) in 3 mL water were stirred at 100 °C for an appropriate time (Table 4). The progress of the reaction was monitored by TLC. After completion of the reaction, the mixture was cooled to room temperature and poured into H_2O (10 ml), and extracted with CH_2Cl_2 (2 × 5 ml) to separate the catalyst from the product by magnetic decantation. After extraction, the organic layer was dried over anhydrous Na_2SO_4 and concentrated under reduced pressure; the residue was subjected to column chromatography on silica gel (ethyl acetate and hexane as eluent)

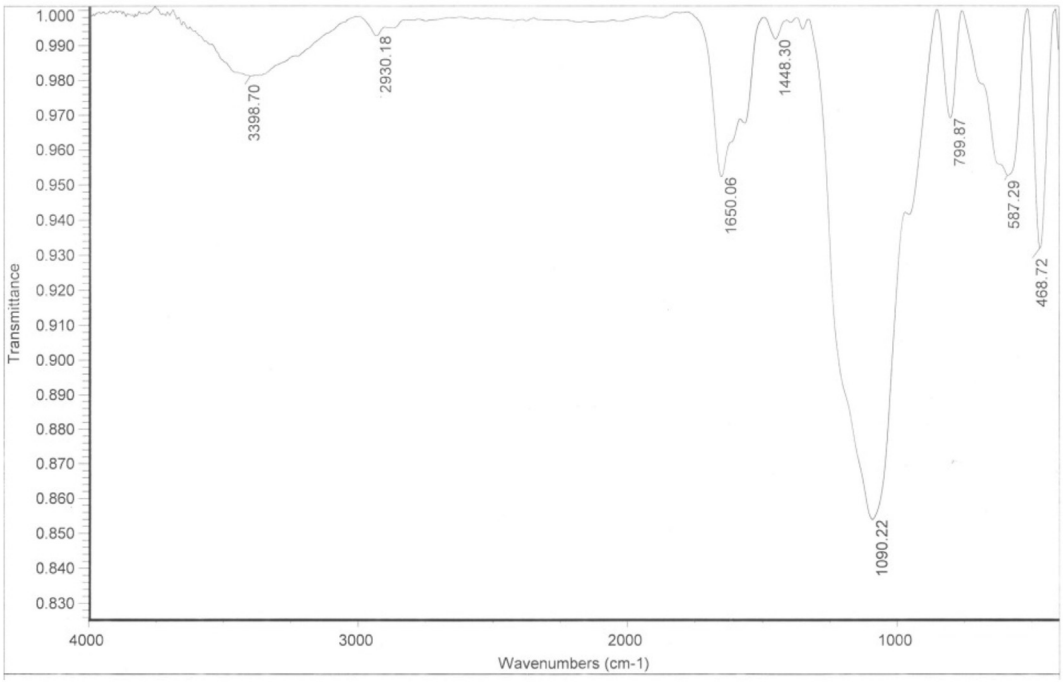

Fig. 1. FT-IR spectrum of the Fe_3O_4@SiO_2@PrNCu magnetic transition-metal catalyst.

to yield the expected pure product. All products were characterized by ^1H and ^{13}C spectra (refer to electronic supporting information).

3. Results and discussion

To prove the preparation of the Fe_3O_4@SiO_2@PrNCu magnetic transition-metal catalyst successfully, the prepared catalyst was characterized by FT-IR (Fig. 1). In detail, in Fig. 1 the strong band appeared at around 587 cm^{-1} corresponded to characteristic peak of Fe–O vibrations in the Fe_3O_4 magnetic nanoparticles [12]. In terms of silica core-shell, Fe_3O_4@SiO_2, the weak band around 800 cm^{-1} in FT-IR spectrum (Fig. 1), which was the characteristic peak of Si–O–Fe, implied that the siliceous polymer network chemically adhered to the bare Fe_3O_4 magnetic nanoparticle surfaces [13]. The absorbing bands at 1090 cm^{-1} and 3398 cm^{-1} can be attributed to the Si–O and N–H respectively [13]. Finally, the weak band at 2930 cm^{-1} was the C–H stretching vibrations of the methylene groups in propyl and that at 1448 cm^{-1} corresponds to bending vibration (Fig. 1). It should be taken into account that the characteristic peaks of Fe_3O_4 and Fe_3O_4@SiO_2 can be observed with

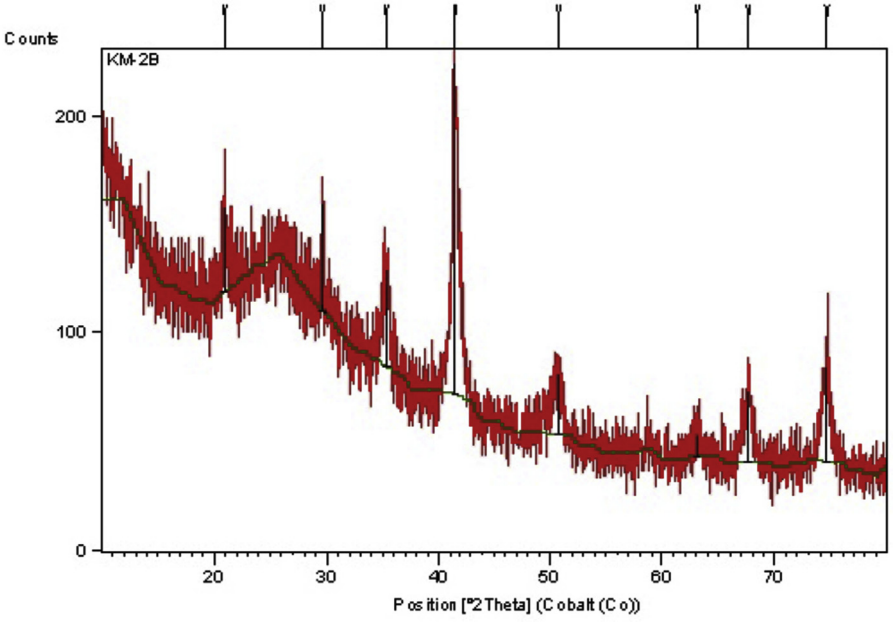

Fig. 2. Powder X-Ray diffraction pattern of the Fe_3O_4@SiO_2@PrNCu magnetic transition-metal catalyst.

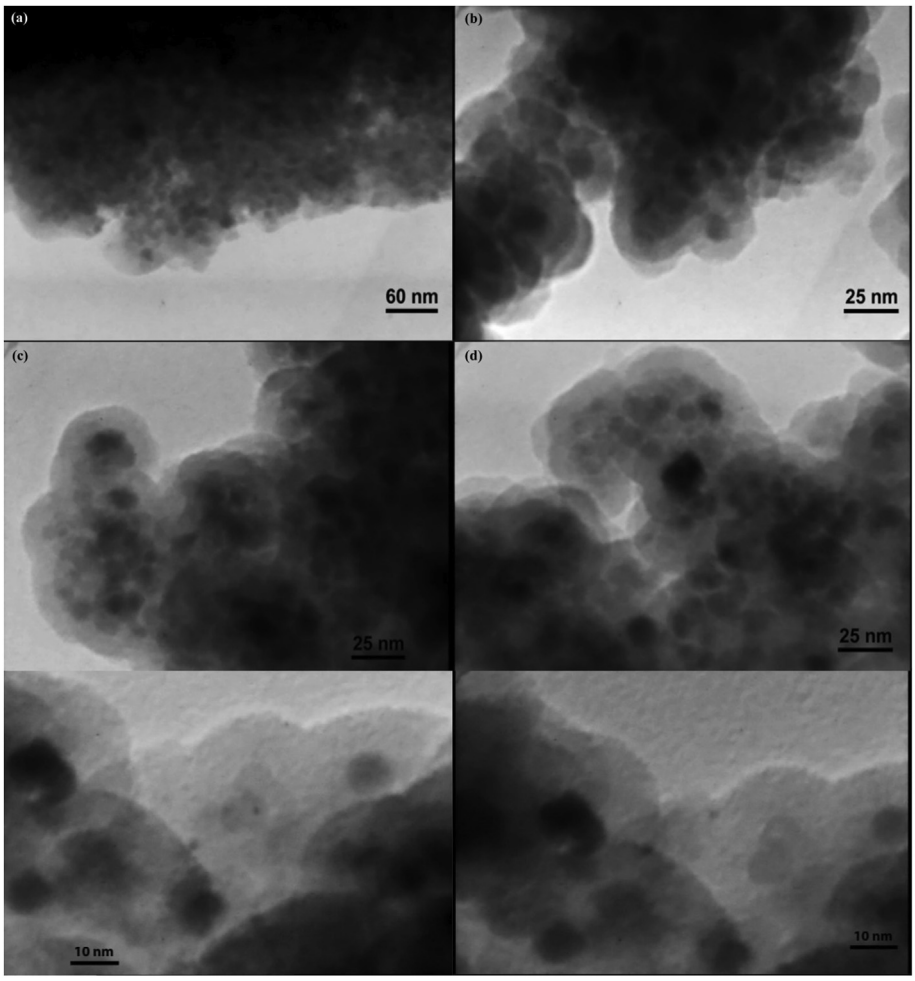

Fig. 3. TEM images of the core-shell Fe_3O_4@SiO_2@PrNCu magnetic transition-metal catalyst at 60, 25 and 10 nm resolutions.

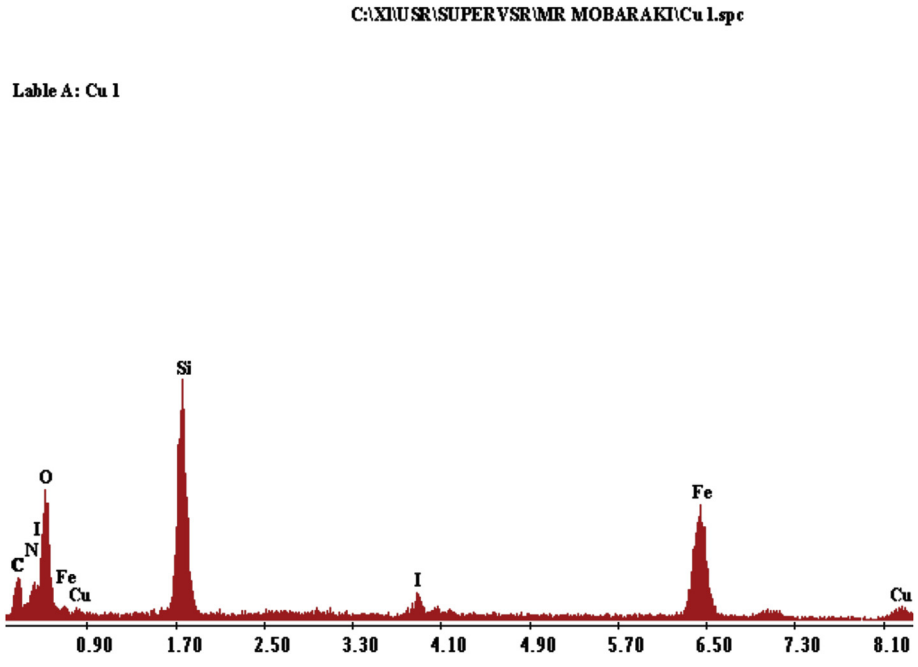

Fig. 4. EDX spectrum of the Fe_3O_4@SiO_2@PrNCu magnetic catalyst.

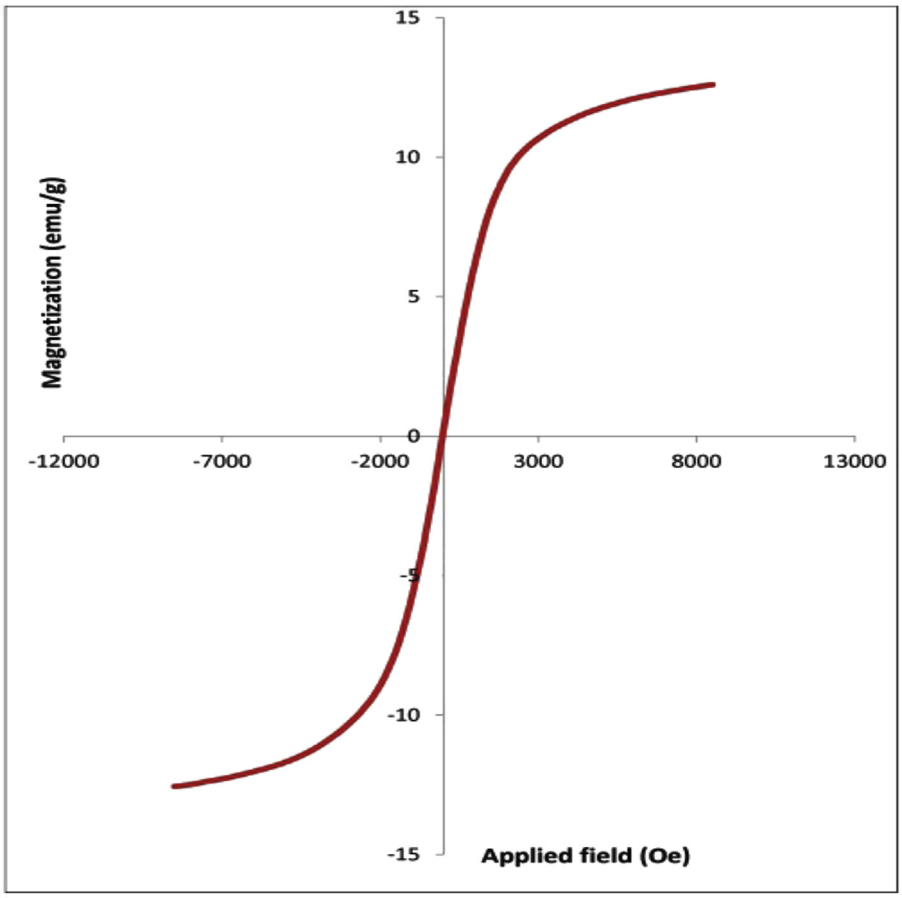

Fig. 5. VSM magnetization curve of the Fe_3O_4@SiO_2@PrNCu magnetic transition-metal catalyst.

a little shift after the modifications. Structural changes were clearly observed after sequence modifications with characteristic peaks of silica core-shell, methylene moieties of propyl group and N–H bond of Guanidine like ligand of the Fe_3O_4@SiO_2@PrNCu magnetic transition-metal catalyst in FT-IR spectrum. This confirmed the successful modification of Fe_3O_4 MNPs with silica shell and TMSPU groups via covalent bonds.

To further verify the successful formation of the magnetic transition-metal catalyst, crystalline structure of the Fe_3O_4@SiO_2@PrNCu was identified with the XRD (Fig. 2). The obtained XRD pattern showed the characteristic diffraction peaks of the nanoparticles at 2θ values of 20.96, 29.64, 35.23, 41.50, 50.71, 63.13, 67.68 and 74.62 which corresponded to the Miller indices values {h k l} of {2 0 0}, {3 1 1}, {4 0 0}, {4 2 2}, {5 1 1}, {4 4 0}, {6 2 0} and {5 3 3} respectively [12].

These values were consistent with the standard XRD data for the lattice planes of the inverse spinel structure of Fe_3O_4 (JCPDS file no. 19–0629) and revealed the retention of the crystalline structure during functionalization of the Fe_3O_4 MNPs with amorphous silicon shell [12]. The broad band around ($2\theta = 25^\circ$) in the catalyst implied the successful coating of the amorphous silica shell around the Fe_3O_4 MNPs cores (Fig. 2) [12].

To investigate the morphology and texture of the catalyst, the resultant magnetic Fe_3O_4@SiO_2@PrNCu was characterized with using TEM images (Fig. 3). It can be observed that the average particle diameter for synthesized Fe_3O_4@SiO_2@PrNCu was approximately 25 nm. Parts b, c and d in Fig. 3 clearly illustrates that the silica shell can be observed as a light area surrounding dark core of Fe_3O_4. Accordingly it clearly reveals the formation of a core-shell structure for Fe_3O_4@SiO_2@PrNCu magnetic catalyst. The particles modified with siliceous precursors showed a slight aggregation, which might have been due to the magnetic dipolar interaction

Table 1
Optimization of the conditions for the Ullmann reaction of iodobenzene[a].

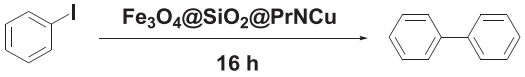

Entry	Cat. (mol%)	Base (mmol)	Temperature (°C)	Solvent	Yield (%)[b]
1	1	K_2CO_3 (3)	100	DMF	52
2	1	Cs_2CO_3 (3)	100	DMF	58
3	1	NEt_3 (3)	100	DMF	25
4	1	NaOAc (3)	100	DMF	50
5	1	Na_2CO_3 (3)	100	DMF	35
6	1	$NaHCO_3$ (3)	100	DMF	25
7	1	K_3PO_4 (3)	100	DMF	70
8	1	K_3PO_4 (3)	100	NMP	93
9	1	K_3PO_4 (3)	100	CH_3CN	60
10	**1**	**K_3PO_4 (3)**	**100**	**H_2O**	**91**
11	1	K_3PO_4 (1)	100	H_2O	15
12	1	K_3PO_4 (2)	100	H_2O	65
13	1	K_3PO_4 (4)	100	H_2O	94
14	1	K_3PO_4 (3)	70	H_2O	60
15	1	K_3PO_4 (3)	85	H_2O	81
16	2	K_3PO_4 (3)	100	H_2O	95
17	1.5	K_3PO_4 (3)	100	H_2O	95
18	0.5	K_3PO_4 (3)	100	H_2O	78

[a] Reaction was carried out using 2 mmol of iodobenzene for 16 h.
[b] Yields refer to the isolated pure products.

Table 2
Ullmann Reaction of various functionalized aryl iodides.

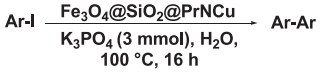

Entry	Aryl halide	product	Yield (%)[a]
1		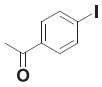	91
2	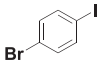	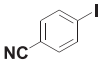	93
3	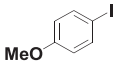	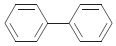	90
4	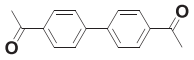	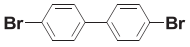	92
5	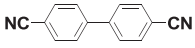	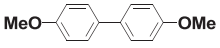	86

[a] Yields refer to the isolated pure products.

among the magnetite Fe_3O_4 NPs.

Furthermore, the composition of the Fe_3O_4@SiO_2@PrNCu magnetic transition-metal catalyst was also confirmed with the EDX analysis experiment (Fig. 4). It reveals the peaks of C, N, I, O, Fe, Si and Cu around 0.25 keV, 0.41 keV, 0.51 and 3.95 keV, 0.65 keV, 0.72 and 6.42 keV, 1.75 keV and finally 0.95 and 8.1 keV respectively. The weight ratios were: C, 12.10%; N, 11.09%; I, 6.42%; O, 20.62%; Fe, 19.29%; Si, 24.41% and Cu, 6.09%. EDX results verify that the carbon, nitrogen and copper atoms are on the surface of Fe_3O_4@SiO_2@PrNCu magnetic catalyst, which indicates that guanidine-like ligand-metal complex, is successfully grafted on the surface of Fe_3O_4@SiO_2 core-shell MNPs.

The magnetic property of the catalyst is very suitable for easy removal and recovery of that from the reaction medium. To evaluate the magnetic property of the obtained catalyst, vibrating sample magnetometer (VSM) measurement at room temperature was performed (Fig. 5). As Fig. 5 illustrates, a 12.4 emu/g saturation magnetization (Ms) was achieved and no hysteresis was present in the magnetization curve, which indicated that the magnetic particles of the catalyst were superparamagnetic. Thus, the prepared catalyst is removed easily from the reaction medium with a simple magnet due to their superparamagnetism and sufficient saturation magnetization.

For the beginning of this study, the catalytic performance of the Fe_3O_4@SiO_2@PrNCu was tested in the Ullmann carbon–carbon coupling reaction. To find the best reaction conditions, our investigation was initiated between 2 mol of iodobenzenes molecules in the presence of K_2CO_3 (3 mmol), N,N-dimethylformamide (DMF) and Fe_3O_4@SiO_2@PrNCu (1 mol%) magnetic transition-metal catalyst as a model reaction at 100 °C for 16 h, thus affording 52% isolated yield for Biphenyl (Table 1, entry 1). To probe the effect of various conditions, the effect of different bases, temperature, and solvents was screened using Fe_3O_4@SiO_2@PrNCu as the magnetic transition-metal catalyst (Table 1). Firstly, the effect of various bases with constant loading of the catalyst (1 mol%) and DMF as the solvent at 100 °C for 16 h was examined (Table 1, entries 1–7). A considerable increase in the product formation was found in the presence of K_3PO_4 (3 mmol) as the base (Table 1, entry 7). Under these similar conditions, different solvents including N-methylpyrrolidone (NMP), H_2O and CH_3CN were explored. The yield of the reaction was raised at the presence of NMP and H_2O solvents; so to work in green condition we used H_2O as the optimized solvent (Table 1, entries 7–10). Also, other base concentrations (1, 2, and 4 mmol) were surveyed under similar reaction conditions (Table 1, entries 11–13); among them, 3 mmol of the K_3PO_4 was selected as optimal amount (Table 1, entry 10). It was revealed that reducing the reaction temperature from 100 °C to lower temperatures (85 and 70 °C) had a negative effect on the product yield (Table 1, entries 14, 15). Finally, different loadings of the catalyst were investigated (Table 1, entries 16–18); among them, 1 mol% of the catalyst was found to be the best (Table 1, entry 10). Increasing the amount of the catalyst did not have any significant impact on the product yield but reducing the amount of the catalyst gave the desired product in a lower yield at the same reaction conditions. Therefore, it displays considerable effect of the catalyst in the reaction progress. It was concluded that the optimized condition for this reaction is 1 mol% of the catalyst, 3 mmol of the K_3PO_4 as the base and H_2O as a green solvent at 100 °C (Table 1, entry 10).

Table 3
Optimization of the conditions for the Mizoroki-Heck reaction of bromobenzene with ethylacrylate[a].

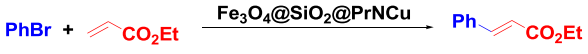

Entry	Cat. (mol%)	Base (mmol)	Temperature (°C)	Time (h)	Solvent	Yield (%)[b]
1[c]	1	K_3PO_4 (3)	100	16	H_2O	<10
2	0.5	K_3PO_4 (3)	100	16	H_2O	95
3	0.5	K_3PO_4 (2)	100	16	H_2O	93
4	0.5	K_3PO_4 (1)	100	16	H_2O	87
5	0.5	K_3PO_4 (0.5)	100	16	H_2O	75
6	0.1	K_3PO_4 (2)	100	24	H_2O	83
7	0.2	K_3PO_4 (2)	100	16	H_2O	91
8	0.3	K_3PO_4 (2)	100	16	H_2O	92
9	0.2	K_3PO_4 (2)	50	24	H_2O	<5
10	0.2	K_3PO_4 (2)	70	16	H_2O	45
11	0.2	K_3PO_4 (2)	85	16	H_2O	81
12	0.2	K_3PO_4 (2)	100	16	NMP	65
13	0.2	K_3PO_4 (2)	100	16	DMSO	52
14	0.2	K_3PO_4 (2)	100	16	DMF	68
15	0.2	K_3PO_4 (2)	100	16	THF	73

[a] Reaction conditions: bromobenzene (1 mmol), ethyl acrylate (1.2 mmol) and TBAB (0.5 mmol).
[b] Yields refer to the isolated pure products.
[c] Reaction was carried out without presence of TBAB.

The utility of the procedure was extended by coupling various aryl halides under the optimized conditions. The results are summarized in Table 2. 4-Iodoacetophenone, 4-Iodobromobenzene and 4-Iodobenzonitrile successfully produced the expected products in excellent yields (Table 2, entries 2–4). 4-methoxyIodobenzene (Table 2, entry 5) produced the desired products in good yield, indicating both electron-donating as well as electron-withdrawing substituents on the iodobenzene ring were tolerated and worked well to give the corresponding biaryls under the optimized conditions.

Among transition-metals, palladium was largely utilized as catalyst in Mizoroki-Heck carbon-carbon coupling reaction between aryl halides with olefins. In other words, palladium catalysis and Mizoroki-Heck reaction both are so closely dependent and are intimate parts of transition-metal catalyzed carbon-carbon bond-forming reactions [14]. Although, there are many developments of palladium-catalyzed Mizoroki-Heck carbon-carbon bond formation during the last three decades, these methodologies have some

Table 4
Catalytic Mizoroki-Heck reactions of various aryl halides with olefins[a].

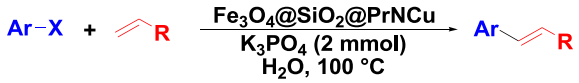

Entry	Cat. (mol%)	Ar-X	R	Time (h)	TBAB (mmol)	Yield (%)[b]
1	0.2	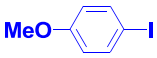	CO_2Et	10	-	97
2	0.2	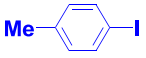	CO_2Et	8	-	94
3	0.2	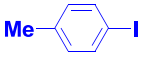	Ph	12	-	91
4	0.2	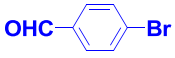	CO_2Et	10	-	93
5	0.2	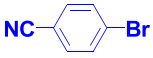	CO_2Et	10	-	92
6	0.2	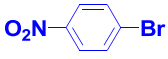	CO_2Et	8	-	92
7	0.2	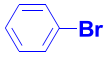	CO_2Et	16	0.5	91
8	0.2	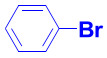	Ph	20	0.5	85
9	0.2		Ph	20	0.5	79
10	0.2	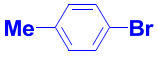	CO_2Et	24	1	90
11	0.2	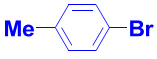	Ph	24	1	66
12	0.2	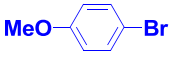	CO_2Et	24	1	85
13	0.2	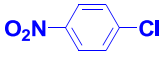	CO_2Et	24	1	79
14	0.2	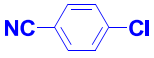	CO_2Et	24	1	69
15	0.5	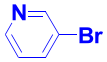	CO_2Et	24	1	75
16	0.5	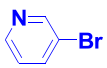	CO_2Bu	24	1	69
17	0.5		CO_2Et	24	1	89
18	0.5		CO_2Bu	24	1	87

[a] Reaction conditions: bromobenzene (1 mmol) and ethyl acrylate (1.2 mmol).
[b] Yields refer to the isolated pure products.

drawbacks [15]. Such drawbacks include but are not limited to the cost of palladium as an expensive metal and the removal of the trace contamination of the intermediates and product by palladium leaching. Taking into account the economy and safety product of this reaction, the recovery of the costly Pd catalyst is required primarily and then the use of cheaper metals as catalyst, which could replace or complement the palladium catalytic systems, is a remarkable task as well. So, the easy separation and recovery of magnetic catalysts with a simple magnet which prevent any remnant of palladium in the reaction medium, offer an effective solution [16]; and also, among transition-metals the use of copper and copper based catalysts as alternative to palladium is an attractive research target for many groups. So many researchers turn their attention to the copper due to eco-friendly and low-cost aspect of copper [17]. It is obvious that utilization of copper as an alternative catalyst is much cheaper than other transition metal catalysts, thus it has been used in many coupling reactions but to our knowledge, there is no systematic study in the literature present to elaborate and investigate the effectiveness of magnetite-based copper catalyst applied to catalyzed Mizoroki-Heck carbon-carbon coupling reaction.

In this regard, and as part of our efforts in surveying magnetic materials in organic transformations [18], we have designed and utilized copper heterogeneous magnetic based catalyst (Fe_3O_4@-SiO_2@PrNCu) (Scheme 1) in the Mizoroki-Heck carbon-carbon coupling reaction as the main part of this report.

The aforementioned optimized conditions for the Ullmann coupling reaction were not successful when Fe_3O_4@SiO_2@PrNCu was used in the Mizoroki-Heck reaction of bromobenzene (1 mmol) with ethyl acrylate (1.2 mmol) (Table 3, entry 1). Therefore, to found the optimized reaction conditions an additive, a quaternary ammonium salt promoter, was added and the model reaction was performed between bromobenzene (1 mmol) and ethyl acrylate (1.2 mmol) in the presence of Fe_3O_4@SiO_2@PrNCu (0.5 mol%), TBAB (0.5 mmol), K_3PO_4 (3 mmol) and H_2O as solvent for 16 h at 100 °C (Table 3, entry 2). Following our investigations, to find the optimized reaction conditions, other parameters such as the effect of different amounts of catalyst, base, temperature and other types of solvents were studied. In the presence of lower values of K_3PO_4 as an inorganic base a considerable decrease in the product formation was observed (Table 3, entries 3–5). Also, different mol% of the Fe_3O_4@SiO_2@PrNCu (0.1, 0.2 and 0.3 mol%) were screened (Table 3, entries 6–8); among them, 0.2 mol% of the catalyst was found to be the best (Table 3, entry 7). Obviously, reducing the reaction temperature from 100 °C to lower temperatures (85, 70 and 50 °C) had a negative effect on the product yields (Table 3, entries 9–11). Also, we surveyed other kinds of solvents including NMP, DMSO, DMF and THF (Table 3, entries 12–15). Therefore, the yield of the coupled product was more satisfactory when K_3PO_4 (2 mmol) as the base, H_2O as the solvent and 0.2 mol% of the catalyst at 100 °C as the optimum conditions were employed (Table 3, entry 7).

With the optimized reaction conditions in hand, the efficiency of the procedure was further extended by coupling various aryl halides with olefins (Table 4). As anticipated, the reaction of aryl iodides with ethyl acrylate and styrene even in the absence of TBAB, reactions progressed very smoothly to give the desired products in 90–97% isolated yields (Table 4, entries 1–3). A wide range of substituted aryl bromides, with both electron-rich and electron-deficient substituents, worked well with olefins to give the corresponding products in high to excellent yields. Under the same reaction conditions used for aryl iodides, aryl bromides with an electron-withdrawing group in the para position were more reactive in comparison to those with an electron-donating group (Table 4, entries 4–6). Coupling of bromobenzene and electron-rich aryl bromides with ethyl acrylate and styrene substrates gave poor yields; therefore, tetrabutylammonium bromide (TBAB, 0.5–1 mmol) was added as a promoter to the reaction mixture (Table 4, entries 7–12). Due to lower reactivity of aryl chloride and catalyst poisoning character of heteroaryl halides corresponding products with lower yields were produced (Table 4, entries 13–18).

Heterogeneous catalytic nature and copper leaching of the catalyst were investigated with the hot-filtration-like experiment for the Mizoroki-Heck reaction of iodobenzene with ethyl acrylate in the presence of 0.2 mol% of the catalyst, 2 mmol of the K_3PO_4 as the base and H_2O as the green solvent at 100 °C. After 2 h the catalyst was removed easily from the reaction medium with a simple magnet due to its superparamagnetism (7% conversion) (Fig. 6). The catalyst free portion of the reaction which was decanted was further stirred for another 14 h but gave almost no conversion (2% conversion), indicating an extremely low metal leaching from the support. This could be attributed to the ligand design which includes nitrogen donor sets, which leads to more coordination of the ligand to the metal and good metal–ligand interaction. So this makes the catalyst highly stable under the reaction conditions and minimizes catalyst deterioration and copper leaching and finally allows efficient catalyst recycling. These observations led the authors to conclude on a truly heterogeneous catalysis.

To more approve the leaching-test results, heterogeneity and reusability of the catalyst, the recovery of the Fe_3O_4@SiO_2@PrNCu catalyst (0.2 mol%) in the Mizoroki-Heck coupling of bromobenzene with ethyl acrylate in the presence of TBAB (0.5 mmol), K_3PO_4 (2 mmol) as base and H_2O as solvent at 100 °C for 16 h was tested. Upon completion of the first reaction to yield the corresponding product, the catalyst was easily separated and recovered from the reaction mixture by an external magnet, washed with ethanol and finally dried under vacuum prior to the next run. During the recycling experiment with fresh reactants, under the same reaction conditions, minor change in the catalytic activity was observed for at least six consecutive runs which clearly demonstrate the stability of the catalyst for these reaction conditions (Fig. 7).

4. Conclusions

In summary, this paper has brought into our attention a preparation procedure of a novel magnetic transition-metal catalyst through co-precipitation and sol-gel experimental methods for application in carbon-carbon coupling reactions.

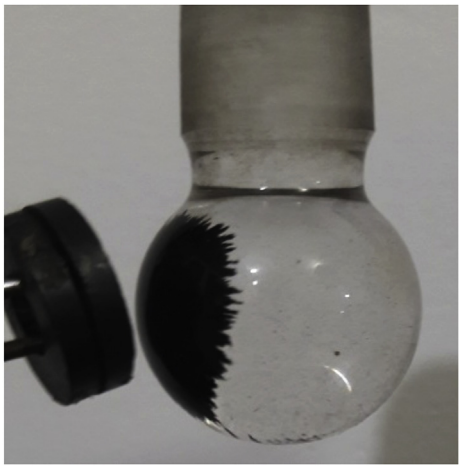

Fig. 6. Photograph of separation of the catalyst with a simple magnet.

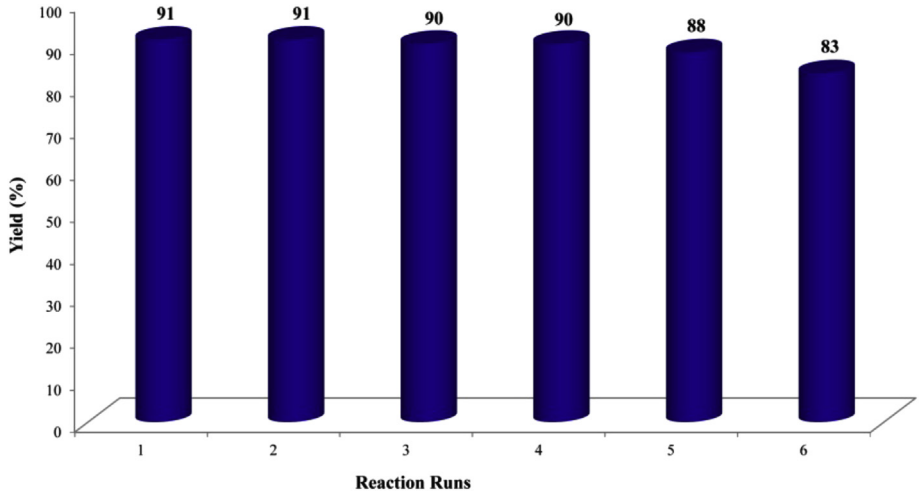

Fig. 7. Recyclability of the Fe_3O_4@SiO_2@PrNCu catalyst for the Mizoroki-Heck carbon-carbon coupling reaction.

Magnetic behaviour of the catalyst besides the use of an electron-rich guanidine like bidentate ligand in the structure of catalyst improve the recovery and reusability of the catalyst and prevent any leaching of the transition metal active sites. In other words, the NH moieties on the surfaces of the catalyst has shown high affinity for transition metal nanoparticles and the geminal nitrogen of the NH_2 moieties show electron donating properties which provides an electron-rich bidentate ligand to produce a more stable complex with N-donor coordination sites. Also, the large surface area of the Fe_3O_4@SiO_2 core-shell magnetic nanoparticles caused higher loading of the copper transition metal active sites and produced a more robust catalyst. Furthermore, this study highlights the value of replacing precious metal catalyst with a cheaper and more sustainable one. Therefore, this work represents Fe_3O_4@SiO_2@PrNCu magnetic catalyst including Cu active sites as an inexpensive and eco-friendly alternative to Pd-based catalytic system for Mizoroki-Heck carbon-carbon coupling reaction. So far we have come to this conclusion that Fe_3O_4@SiO_2@PrNCu magnetic transition metal catalyst is a multipurpose alternative catalyst for performing of the coupling reactions due to its special characteristics including saving cost, ease of both preparation and separation, evenness in particle distribution, efficient activity as well as basicity and fine nanosize particles.

Acknowledgment

This work was supported by the Research Council of the Tarbiat Modares University and the Iran National Science Foundation (INSF, Grant No. 94028939).

Appendix A. Supplementary data

Supplementary data to this article can be found online at https://doi.org/10.1016/j.jorganchem.2019.06.029.

References

[1] L. Yin, J. Liebscher, Chem. Rev. 107 (2007) 133–173.
[2] (a) A.F.P. Biajoli, C.S. Schwalm, J. Limberger, T.S. Claudino, A.L. Monteiro, J. Braz. Chem. Soc. 25 (2014) 2186–2214;
(b) Q. Yang, H. Jin, Y. Xu, P. Wang, X. Liang, Z. Shen, Z. Chen, D. Zou, X. Fan, Q. Zhou, Macromolecules 42 (2009) 1037–1046;
(c) V.L. Budarin, P.S. Shuttleworth, J.H. Clark, R. Luque, Curr. Org. Synth. 7 (2010) 614–627.
[3] (a) C. Torborg, M. Beller, Adv. Synth. Catal. 351 (2009) 3027–3043;
(b) T.-S. Jo, S.H. Kim, J. Shin, C. Bae, J. Am. Chem. Soc. 131 (2009) 1656–1657.
[4] (a) X. Liu, X. Wen, R. Hoffmann, ACS Catal. 8 (2018) 3365–3375;
(b) R. Narayanan, M.A. El-Sayed, J. Phys. Chem. B 109 (2005) 12663–12676;
(c) L.D. Pachon, G. Rothenberg, Appl. Organomet. Chem. 22 (2008) 288–299.
[5] (a) I.P. Beletskaya, A.V. Cheprakov, Coord. Chem. Rev. 248 (2004) 2337–2364;
(b) S.V. Ley, A.W. Thomas, Angew. Chem. Int. Ed. 42 (2003) 5400–5449;
(c) K. Kunz, U. Scholz, D. Ganzer, Synlett (2003) 2428–2439;
(d) F. Monnier, M. Taillefer, Angew. Chem. Int. Ed. 47 (2008) 3096–3099;
(e) G. Evano, N. Blanchard, M. Toumi, Chem. Rev. 108 (2008) 3054–3131;
(f) A. Klapars, X. Huang, S.L. Buchwald, J. Am. Chem. Soc. 124 (2002) 7421–7428;
(g) J.C. Antilla, A. Klapars, S.L. Buchwald, J. Am. Chem. Soc. 124 (2002) 11684–11688;
(h) F.Y. Kwong, S.L. Buchwald, Org. Lett. 5 (2003) 793–796;
(i) D. Ma, Q. Cai, H. Zhang, Org. Lett. 5 (2003) 2453–2455;
(j) B. de Lange, M.H. Lambers-Verstappen, L.S. de Vondervoort, N. Sereinig, R. de Rijk, A.H.M. de Vries, J.G. de Vries, Synlett (2006) 3105–3109;
(k) A. Shafir, S.L. Buchwald, J. Am. Chem. Soc. 128 (2006) 8742–8743;
(l) A. Ouali, J.-F. Spindler, A. Jutand, M. Taillefer, Organometallics 26 (2007) 65–74.
[6] (a) R.B.N. Baig, R.S. Varma, Chem. Commun. 49 (2013) 752–770;
(b) Q. Dong, Zh Meng, Ch-L. Ho, H. Guo, W. Yang, I. Manners, L. Xu, W.-Y. Wong, Chem. Soc. Rev. 47 (2018) 4934–4953;
(c) Zh Meng, G. Li, H.-F. Wong, Sh-M. Ng, S.-Ch Yiu, Ch-L. Ho, Ch-W. Leung, I. Manners, W.-Y. Wong, Nanoscale 9 (2017) 731–738;
(d) Zh Meng, Ch-L. Ho, H.-F. Wong, Zh-Q. Yu, N. Zhu, G. Li, Ch-W. Leung, W.-Y. Wong, Sci. China. Mater. 62 (2019) 566–576;
(e) Zh Meng, G. Li, N. Zhu, Ch-L. Ho, Ch-W. Leung, W.-Y. Wong, J. Organomet. Chem. 849–850 (2017) 10–16;
(f) Q. Dong, G. Li, Ch-L. Ho, Ch-W. Leung, PhW.-T. Pong, I. Manners, W.-Y. Wong, Adv. Funct. Mater. 24 (2014) 857–862;
(g) Q. Dong, G. Li, Ch-L. Ho, M. Faisal, Ch-W. Leung, PhW.-T. Pong, K. Liu, B.-Zh Tang, I. Manners, W.-Y. Wong, Adv. Mater. 24 (2012) 1034–1040;
(h) K. Liu, Ch-L. Ho, S. Aouba, Y.-Q. Zhao, Zh-H. Lu, S. Petrov, N. Coombs, P. Dube, H.E. Ruda, W.-Y. Wong, I. Manners, Angew. Chem. Int. Ed. 47 (2008) 1255–1259.
[7] V. Polshettiwar, R. Luque, A. Fihri, H. Zhu, M. Bouhrara, J.M. Basset, Chem. Rev. 111 (2011) 3036–3075.
[8] S. Shylesh, V. Schnemann, W.R. Thiel, Angew. Chem. Int. Ed. 49 (2010) 3428–3459.
[9] G. Evano, N. Blanchard, Copper-Mediated Cross-Coupling Reactions, John Wiley & Sons, Inc., 2014.
[10] (a) C. Sambiagio, S.P. Marsden, A.J. Blackera, P.C. McGowan, Chem. Soc. Rev. 43 (2014) 3525–3550;
(b) H. Lin, D. Sun, Org. Prep. Proced. Int. 45 (2013) 341–394;
(c) S. Monda, ChemTexts 17 (2016) 1–11.
[11] (a) B.W. Crabbe, O.P. Kuehm, J.C. Bennett, G.L. Hallett-Tapley, Catal. Sci. Technol. 8 (2018) 4907–4915;
(b) A. Gao, H. Liu, L. Hu, H. Zhang, A. Hou, K. Xie, Chin. Chem. Lett. 29 (2018) 1301–1304;
(c) N. Marina, A.E. Lanterna, J.C. Scaiano, ACS Catal. 8 (2018) 7593–7597;
(d) N.K. Ojha, G.V. Zyryanov, A. Majee, V.N. Charushin, O.N. Chupakhin, S. Santra, Coord. Chem. Rev. 353 (2017) 1–57;
(e) B. Zhu, L.K. Yan, L.S. Yao, H. Ren, R.H. Li, W. Guan, Z.M. Su, Chem. Commun. 54 (2018) 7959–7962.
[12] Q. Zhang, H. Su, J. Luo, Y. Wei, Green Chem. 14 (2012) 201–208.
[13] W. Li, B. Zhang, X. Li, H. Zhang, Q. Zhang, Appl. Catal. Gen. 459 (2013) 65–72.
[14] (a) C.C.C.J. Seechurn, M.O. Kitching, T.J. Colacot, V. Snieckus, Angew. Chem. Int.

Ed. 51 (2012) 5062–5085;
(b) M. Lamblin, L. Nassar-Hardy, J.C. Hierso, E. Fouquet, F.X. Felpin, Adv. Synth. Catal. 352 (2010) 33–79;
(c) I.P. Beletskaya, A.V. Cheprakov, Chem. Rev. 100 (2000) 3009–3066;
(d) A. Kumar, G.K. Rao, S. Kumar, A.K. Singh, Organometallics 33 (2014) 2921–2943;
(e) A. Biffis, P. Centomo, A.D. Zotto, M. Zecca, Chem. Rev. 118 (2018) 2249–2295;
(f) A. Molnar, Chem. Rev. 111 (2011) 2251–2320;
(g) J. Ruan, J.A. Iggo, J. Xiao, J. Organomet. Chem. 880 (2019) 150–155;
(h) M. Khajehzadeh, M. Moghadam, J. Organomet. Chem. 863 (2018) 60–69.
[15] (a) L. Fernández-García, M. Blanco, C. Blanco, P. Álvarez, M. Granda, R. Santamaría, R. Menéndez, J. Mol. Catal. A Chem. 416 (2016) 140–146;
(b) B. Movassagh, Sh Ranjbari, Appl. Organomet. Chem. 32 (2018) 1–6.
[16] (a) B.S. Kumar, R. Anbarasan, A.J. Amali, K. Pitchumani, Tetrahedron Lett. 58 (2017) 3276–3282;
(b) M. Nikoorazm, F. Ghorbani, A. Ghorbani-Choghamarani, Z. Erfani, Appl. Organomet. Chem. 32 (2018) 1–13;
(c) J. Li, Y. Wang, Sh Jiang, H. Zhang, J. Organomet. Chem. 878 (2018) 84–95.
[17] (a) V. Calo, A. Nacci, A. Monopoli, E. Ieva, N. Cioffi, Org. Lett. 7 (2005) 617–620;
(b) Y. Peng, J. Chen, J. Ding, M. Liu, W. Gao, H. Wu, Synthesis 2 (2011) 213–216;
(c) A. Faulkner, N.J. Race, J.S. Scott, J.F. Bower, Chem. Sci. 5 (2014) 2416–2421;
(d) S. Iyer, V.V. Thakur, J. Mol. Catal. A Chem. 157 (2000) 275–278;
(e) V. Declerck, J. Martinez, F. Lamaty, Synlett 18 (2006) 3029–3032.
[18] A. Mobaraki, B. Movassagh, B. Karimi, ACS Comb. Sci. 16 (2014) 352–358.